Separation of Reflection Components for Measured Spectral BRDFs

Category: Research

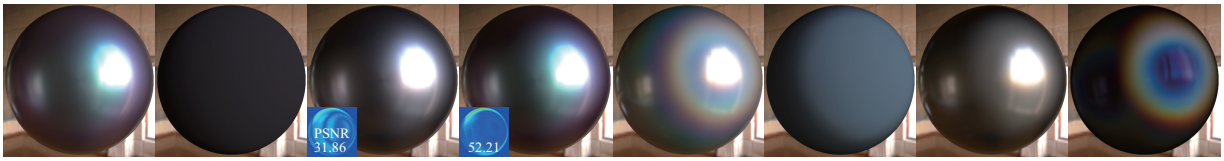

Figure 1: Diffuse specular separation of measured spectral BRDFs. (a) reference image of cc_nothern_aurora material. (b) the diffuse component of (a). The specular components separated by using (c) the previous method [26] and (d) our method. Our method can represent the color-changing effects, while the previous method fails to represent goniochromatic effects. The inset images show the mean absolute errors (MAPEs) and peak signal-to-noise ratio (PSNR). (e) reference image of iris_flake_paint2 material. (f) the diffuse component of (e). (g) and (h) are the specular components of (e), and (g) shows the Fresnel effect that depends only on the difference angle θ_d between the incident direction and the half vector. In contrast, (h) shows the diffraction effect that depends on the difference angle θ_d and the half angle θ_h between the half vector and the normal. As shown in these images, our method can separate three reflection components with different properties.

Abstract

Measured BRDFs, which are acquired by measuring the reflectance of real-world materials, can reproduce the material appearance faithfully. The measured reflectance is a mixture of reflection components with different properties, such as diffuse reflections and specular reflections. However, recent applications, including light-probe rendering and denoising often require the separated representation of BRDFs to apply each component to different pipelines for efficient rendering. This paper proposes a separation method of isotropic measured spectral BRDFs to handle goniochromatic effects based on the spectral microfacet BRDF and diffraction microfacet BRDF models. Experimental results show that our method can increase the PSNR to about 30 dB compared with the previous method.

Index Terms: Computing methodologies—Computer graphics—Rendering—Reflectance Modeling;

1 Introduction

Bidirectional Reflectance Distribution Functions (BRDFs) are a basis for modeling the reflectance of object surfaces and can be categorized into analytic and data-driven models. Analytic model approximates BRDFs with a parametric model with few parameters. A data-driven model (also known as measured BRDF) uses the acquired reflectance data of real-world materials to represent BRDFs. Several measured BRDF datasets such as MERL BRDF [20] and UTIA BRDF [9], have been used pervasively. In recent years, Dupuy and Jakob proposed an efficient acquisition method of spectral reflectances of real-world materials, EPFL BRDF [8]. Using the measured spectral BRDFs makes it possible to achieve accurate color reproduction, such as iridescence and fluorescent colors, which was difficult with conventional RGB BRDFs.

Rendering applications such as precomputed radiance transfer [29], light probe rendering [11], and denoising [2] often require separating the reflectance into diffuse and specular reflections to apply each component to different rendering pipelines for efficiency. For analytic BRDF models, the diffuse and the specular components are separated from the beginning. Measured BRDFs, on the other hand, consist of a mixture of different reflection components, and the diffuse-specular separation of measured BRDFs is more involved than analytic models.

To address this problem, Sun et al. proposed a diffuse-specular separation method for MERL BRDFs [26]. This method separates each measured BRDF into diffuse and specular components, each represented by the product of a *single* RGB color component and the directional component. Therefore, this method fails to represent materials exhibiting iridescent and diffraction effects that can change colors depending on the incident/outgoing directions.

This paper proposes a method that can separate isotropic measured spectral BRDFs into reflection components with different properties. Our method first separates each measured BRDF into the diffuse and the specular components. To handle materials exhibiting goniochromatic effects, our method represents the specular component with the product of a direction-dependent term and a term that depends on direction and wavelength. By assuming the diffraction model proposed by Holzschuch and Pacanowski [12], our method further separates the specular component into the Fresnel and diffraction effects. Compared with the previous separation method [26], the proposed method can improve PSNR (Peak Signal-to-Noise Ratio) by up to 30 dB.

The contributions of our method can be summarized as follows:

- we propose a diffuse-specular separation method capable of reproducing the goniochromatic effects.
- we further separate the specular component into the Fresnel and diffraction effects.
- we will publicize the source code and the separated data to ensure reproducibility.

2 Related Work

Data-driven BRDF models. Matusik et al. measured the reflectances of 100 real-world isotropic materials [20]. Filip and Vavra measured anisotropic reflectances such as fabrics and leather [9]. Dupuy and Jakob proposed an efficient acquisition method for isotropic and anisotropic materials [8]. By measuring a full spectrum of real-world materials, the EPFL BRDF dataset includes a rich set of materials exhibiting iridescent effects. While using measured BRDFs can enhance realism, *raw* measured BRDFs that mix different reflection components (e.g., diffuse and specular) prevent us from using several rendering applications [2, 11] requiring separated reflection components.

Analytical BRDF fitting. Since the storage of measured BRDFs is relatively large, attempts to fit with analytic BRDF models have been made to MERL BRDF dataset. Ngan et al. fitted several analytic BRDF models (e.g., Cook-Torrance BRDF) to

the MERL BRDF dataset [22]. Several BRDF models, such as ABC models [19], Shifted Gamma microfacet distribution [1], student's t-distribution [24], and two-scale microfacet reflectance model [12], use MERL BRDF dataset as the benchmark to demonstrate the expressiveness of each BRDF model. Bieron and Peers proposed a two-stage image-based fitting for Cook-Torrance and GGX microfacet BRDF models [4]. These methods require costly non-linear optimizations for fitting, and obtaining optimized parameter values without getting local minima is difficult. Dupuy et al. proposed a technique to extract microfacet BRDF parameters from MERL BRDFs without solving costly and unstable non-linear optimizations [7]. While this method is stable and robust, the extracted parameters are sometimes suboptimal.

BRDF factorization. Factoring 4D BRDFs into lower dimensional factors has been proposed for interactive rendering [14, 16, 21], importance sampling [18], editing spatially-varying BRDFs [17], and compact representation using Tensor decomposition [5]. Nielsen et al. decomposed MERL BRDFs into five principal components, which are interpreted as specular peak, diffuse, specular shape, and Fresnel effects [23]. Bagher et al. proposed a non-parametric factor representation for isotropic RGB BRDFs [1]. The most relevant work to our method is the diffuse-specular separation method proposed by Sun et al. [26]. The separation model represents the diffuse and the specular components with the product of a single color term and a direction-dependent term. Therefore, this separation model cannot handle goniochromatic effects where the color changes with respect to the incident/outgoing directions.

The computer vision community extensively researched image-based methods for separating diffuse and specular components (e.g., [10]). These methods focus on decomposing an input image into several components, while our approach aims to decompose measured BRDF.

Neural BRDF representation. In recent years, measured BRDFs can be represented compactly using neural network [13, 27, 30] and Gaussian Process [25]. These methods represent isotropic RGB BRDFs with low-dimensional latent vectors. While these methods can represent measured BRDFs very compactly, the aims of these methods differ from ours (i.e., separate reflection components from measured BRDFs), and these methods are orthogonal to ours (the separated components are represented with neural-network for compact representation).

3 Background

3.1 Microfacet BRDF Model

Microfacet BRDF model ρ_M [3,6,28] is represented by the following equation:

$$\rho_M(\omega_i, \omega_o, \lambda) = \frac{F(\theta_d, \lambda) D(\theta_h) G(\theta_i) G(\theta_o)}{4 \cos\theta_i \cos\theta_o}, \quad (1)$$

where ω_i and ω_o are incident/outgoing directions, λ is the wavelength, F is the Fresnel term, D is the normal distribution function, G is the geometric attenuation term (shadowing/masking), θ_i and θ_o are the angles between $\omega_i(\omega_o)$ and the surface normal $\mathbf{n}$. θ_h is the angle between the half vector $\mathbf{h} = \frac{\omega_i + \omega_o}{\|\omega_i + \omega_o\|}$ and the surface normal $\mathbf{n}$, θ_d is the angle between $\mathbf{h}$ and ω_i. The normal distribution function D and the geometry term G depend only on the microfacet geometries, not on the wavelength. On the other hand, the Fresnel term F depends on the difference angle θ_d and the wavelength λ, and controlls the color of the reflected radiance.

3.2 Diffraction Microfacet BRDF Model

Holzschuch and Pacanowski extended the microfacet model to represent the diffraction of light due to the nano-scale geometries whose sizes are comparable to the wavelength [12]. We refer to this model as the *diffraction microfacet model*. This model ρ_D is represented by the weighted sum of the conventional microfacet model ρ_M (in Eq. (1)) and the diffraction microfacet model as:

$$\rho_D = A(\theta_d, \lambda)\rho_M + (1 - A(\theta_d, \lambda)) Q(\omega_i, \omega_o, \lambda) S(\theta_h, \theta_d, \lambda), \quad (2)$$

where the relative importance $A(\theta_d, \lambda)$ is calculated by:

$$A(\theta_d, \lambda) = e^{-(2\pi \frac{\sigma_{rel}}{\lambda}(2\cos\theta_d))^2}, \quad (3)$$

σ_{rel} is a roughness parameter. Q is the color term for diffraction, S is calculated by convolving the scattering function S_{HS} based on Harvey-Shack theory [15], and the normal distribution function D. Holzschuch and Pacanowski derived the diffraction microfaet model by assuming that the scattering function S_{HS} and the normal distribution function D are dominant, and Q varies smoothly. Similar to this derivation, our method considers that the diffraction microfacet model ρ_D largely hinges on θ_d, θ_h, and λ.

3.3 Previous Diffuse-Specular Separation Model

The previous method proposed by Sun et al. [26] separated MERL BRDF $\rho(\omega_i, \omega_o, \lambda)$ into the diffuse component ρ_d and the specular component ρ_s as:

$$\rho(\omega_i, \omega_o, \lambda) \approx \rho_d(\omega_i, \omega_o) c_d(\lambda) + \rho_s(\omega_i, \omega_o) c_s(\lambda), \quad (4)$$

where c_d and c_s are the colors of the diffuse and the specular components. As shown in Eq. (4), since the BRDF is decomposed into the direction-dependent terms ρ_d and ρ_s, and the wavelength-dependent terms c_d and c_s, materials with goniochromatic effects that change colors with different incident/outgoing directions (e.g., color-changing-paint1 in MERL datasets) cannot be separated well.

4 Proposed Method

4.1 Separation model

To support measured BRDFs with goniochromatic effects, we propose two separation models for the specular component, while our method assumes that the diffuse component can be decomposed into the product of the direction-dependent term ρ_d and the wavelength-dependent term $c_d(\lambda)$ in the same way as the previous method [26].

Since the Fresnel term F in Eq. (1) depends on both the angle θ_d and the wavelength λ, the specular component of measured spectral BRDF can be represented by the product of direction-dependent term $\rho_s(\omega_i, \omega_o)$ and the component $s_s(\theta_d, \lambda)$ that depends on both θ_d and λ as:

$$\rho_s^F(\omega_i, \omega_o, \lambda) = \rho_s(\omega_i, \omega_o) s_s(\theta_d, \lambda). \quad (5)$$

Since the diffraction microfacet BRDF model largely depends on θ_h, θ_d, and λ, our method separates the specular component as the following equation:

$$\rho_s^D(\omega_i, \omega_o, \lambda) = \rho_s(\omega_i, \omega_o) s_s(\theta_h, \theta_d, \lambda). \quad (6)$$

We refer to ρ_s^F and ρ_s^D as the Fresnel and diffraction models, respectively. In each model, the spectral-dependent components $s_s(\theta_d, \lambda)$ and $s_s(\theta_h, \theta_d, \lambda)$ are referred to as *spectral distribution*.

The proposed method separates isotropic spectral BRDFs in EPFL datasets into diffuse and specular components. Isotropic measured BRDFs are represented by the Rusinkiewicz coordinate system $(\theta_h, \theta_d, \phi_d)$ and sampled in $p(= 90 \times 90 \times 180)$ directions and $l(= 195)$ wavelengths. Each isotropic material in the EPFL BRDF dataset is represented by a matrix $\mathbf{X} \in \mathbb{R}^{p \times l}$ where j-th row corresponds to the BRDF values of l wavelengths for j-th pair of directions ω_i^j, ω_o^j corresponding to j-th tuple of angles $(\theta_{h,j}, \theta_{d,j}, \phi_{d,j})$, and k-th column corresponds to the BRDF values of k-th wavelength for p different directions.

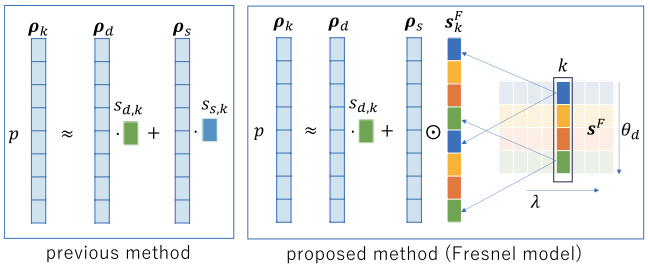

Figure 2: The previous diffuse-specular separation model (left) and our Fresnel model (right). To handle the goniochromatic effects, our method represents the color component with the direction-wavelength dependent component, while the previous method represents the color component independent of the direction component.

4.2 Analytic BRDF fitting

In the first step, the achromatic BRDF $\bar{\rho} \in \mathbb{R}^p$ is calculated by averaging the measured spectral BRDF $\mathbf{X} \in \mathbb{R}^{p \times l}$ across l wavelengths. Then, the achromatic BRDF $\bar{\rho}$ is approximated by the analytic BRDF model $\rho(\alpha) \in \mathbb{R}^p$ (α is a parameter set of the analytic BRDF model). The parameter set α is calculated by solving the following optimization problem:

$$\min_{\alpha_d, \alpha_s} d_1(\bar{\rho}, \rho_d(\alpha_d) + \rho_s(\alpha_s)), \tag{7}$$

$$d_1(\rho_1, \rho_2) = \|\mathbf{g}(\rho_1) - \mathbf{g}(\rho_2)\|_2, \tag{8}$$

where $\mathbf{g} : \mathbb{R}^p \to \mathbb{R}^p$ is a log mapping of j-th component x_j of the argument $\mathbf{x} \in \mathbb{R}^p$ as:

$$g(x_j) = \log(x_j w_j + \varepsilon), \tag{9}$$

$$w_j = \max\{(\mathbf{n} \cdot \omega_i^j)(\mathbf{n} \cdot \omega_o^j), \varepsilon\} \tag{10}$$

where w_j is the weight of the product of cosine terms, and ε is a small constant to avoid singularity ($\varepsilon = 10^{-3}$ is used in our results). $\rho_d(\alpha_d) \in \mathbb{R}^p$ is Lambertian BRDF expressed as:

$$\rho_d(\alpha_d) = \frac{\alpha_d}{\pi} \cdot \mathbf{1}, \tag{11}$$

where α_d is the albedo, $\mathbf{1} \in \mathbb{R}^p$ is a p-dimensional vector whose element is 1. $\rho_s(\alpha_s) \in \mathbb{R}^p$ represents the GGX microfacet BRDF where the j-th component $\rho_{s,j}(\alpha_s)$ corresponds to Eq (1) as:

$$\rho_{s,j}(\alpha_s) = \rho_0 \frac{F(\theta_{d,j}) D(\theta_{h,j}) G(\theta_{i,j}) G(\theta_{o,j})}{4 \cos\theta_{i,j} \cos\theta_{o,j}}, \tag{12}$$

$$F(\theta) = F_0 + (1 - F_0)(1 - \cos\theta)^5, \tag{13}$$

$$D(\theta) = \frac{a^2}{\pi((a^2 - 1)\cos^2\theta + 1)^2}, \tag{14}$$

$$G(\theta) = \frac{2}{1 + \sqrt{1 + a^2 \tan^2\theta}}, \tag{15}$$

where the parameter set α_s consists of the intensity ρ_0, the reflection coefficient at $\theta_d = 0$ F_0, and the roughness parameter a. $\theta_{i,j}, \theta_{o,j}$ are the angles between ω_i^j, ω_o^j and the surface normal $\mathbf{n}$.

4.3 Diffuse-specular separation

In the second step, the achromatic BRDF $\bar{\rho}$ is decomposed into the diffuse component $\rho_d \in \mathbb{R}^p$ and specular components $\rho_s \in \mathbb{R}^p$ by using the analytic BRDF parameters α_d and α_s. Under the condition that the sum of diffuse and specular components is equal to the achromatic BRDF ($\bar{\rho} = \rho_d + \rho_s$), our method calculates the diffuse component ρ_d that minimizes the weighted sum of the differences between each component and the analytic BRDF model:

$$\min_{\rho_d} \eta^d \cdot d_2(\rho_d, \rho_d(\alpha_d)) + \eta^s \cdot d_2(\bar{\rho} - \rho_d, \rho_s(\alpha_s)), \tag{16}$$

$$d_2(\rho_1, \rho_2) = \|(\rho_1 - \rho_2) \odot \mathbf{w}\|_1, \tag{17}$$

where $\mathbf{w} \in \mathbb{R}^p$ consists of the cosine-weight w_j in Eq. (10), $\odot$ represents the Hadamard product, η^d and η^s are weights for each component ($\eta^d = 0.9, \eta^s = 0.8$ are used in our results).

4.4 Restore spectral distributions

Our method restores the spectral distribution $\mathbf{s}$ from the spectral measured BRDF $\mathbf{X}$, the diffuse component ρ_d, and the specular component ρ_s. Our method first restores the diffuse spectral distribution $\mathbf{s}_d \in \mathbb{R}^{1 \times l}$ and the specular spectral distribution $\mathbf{s}_s \in \mathbb{R}^{1 \times l}$ by solving the following optimization problem per wavelength.

$$\min_{s_{d,k}, s_{s,k}} d_1(\rho_k, s_{d,k}\rho_d + s_{s,k}\rho_s), \tag{18}$$

where ρ_k is the k-th column vector of the measured spectral BRDF $\mathbf{X}$, $s_{d,k}$ and $s_{s,k}$ are the k-th component of the diffuse spectral distribution $\mathbf{s}_d$ and the specular spectral distribution $\mathbf{s}_s$, respectively. Once the diffuse spectral distribution $\mathbf{s}_d$ is calculated, the spectral distribution $\mathbf{s}^F \in \mathbb{R}^{90 \times l}$ corresponding to the spectral distribution of Fresnel model $s_s(\theta_d, \lambda)$ in Eq. (5) is calculated by solving the following equation:

$$\min_{\mathbf{s}_k^F} d_1(\rho_k - s_{d,k}\rho_d, \mathbf{s}_k^F \odot \rho_s), \tag{19}$$

where $\mathbf{s}_k^F$ is a p-dimensional vector consists of k-th column of $\mathbf{s}^F$ vertically arranged, as shown in Fig. 2.

Similarly, the spectral distribution $\mathbf{s}^D \in \mathbb{R}^{90^2 \times l}$ corresponding to the spectral distribution $s_s(\theta_d, \theta_d, \lambda)$ of the diffraction model is calculated by:

$$\min_{s_k^D} d_1(\rho_k - s_{d,k}\rho_d, \mathbf{s}_k^D \odot \rho_s), \tag{20}$$

where $\mathbf{s}_k^D \in \mathbb{R}^p$ is a p-dimensional vector consisting of k-th column of $\mathbf{s}^D$ vertically arranged.

4.5 Separation of specular component into Fresnel and diffraction effects

As shown in Eq. (2), the diffraction microfacet BRDF model ρ_D is the sum of the microfacet BRDF model ρ_M whose color is controlled by the Fresnel term F, and the diffraction lobe in which the scattering function $S(\theta_h, \theta_d, \lambda)$ is the dominant factor [12]. To separate the specular component into the Fresnel effect and the diffraction effect, our method subtracts the Fresnel model ρ_s^F from the diffraction model ρ_s^D, and the diffraction effect of the specular component is calculated as:

$$\rho_s(\omega_i, \omega_o)(s_s(\theta_d, \theta_h, \lambda) - s_s(\theta_d, \lambda)). \tag{21}$$

5 Results

We evaluated our two separation models using 51 isotropic spectral BRDFs in the EPFL BRDF dataset. The separation process was performed on a PC with AMD Ryzen Threadripper 3990X CPU. To solve the optimization problem in the first step (Sec. 4.2) and the third step (Sec. 4.4), our method uses the fmincon function in MATLAB, and that in the second step (Sec 4.3) was solved by using the CVXOPT package in Python. The computational time of the diffuse-specular separation is 8.0 min for each material, and that of each step is 2 sec, 3.5 min, and 4.4 min, respectively.

5.1 Diffuse-specular separation

We compare our method with the previous diffuse-specular separation method proposed by Sun et al. [26]. Since the ground truth of each reflection component is unknown for measured BRDFs, we qualitatively evaluate each rendering result and quantitatively evaluate the difference between the sum of two components and the original measured BRDF using relative mean square error (relMSE), mean absolute percentage error (MAPE), peak signal-to-noise ratio (PSNR), and structural similarity index measurement (SSIM).

Table 1 shows the average PSNR, SSIM, MAPE, and relMSE of all isotropic spectral BRDFs in the EPFL BRDF dataset. As shown in Table 1, our Fresnel model improves the average PSNR about 2.1 dB compared to the previous method [26]. Our diffraction model improves that by about 9.5 dB significantly reducing relMSE.

Fig. 3 shows the comparisons of rendered images using (a) the original BRDF, (b) the previous diffuse-specular separation model in Eq. (4), (c) our Fresnel model in Eq. (5), (d) our diffraction model in Eq. (6). As shown in cc_iris_purple_gem (fourth-row) and vch_golden_yellow (eighth-row) materials, our Fresnel model (the third column (c)) can capture the change of colors in highlights, while the previous model fails to capture such effects since the specular color of the previous model is independent of directions. Our diffraction model can represent complex light effects such as cc_blue_agat, irid_flake_paint1, and irid_flake_paint2 materials, where the previous model and our Fresnel model are difficult to reproduce.

Figs. 3(e)(f)(g)(h) show separated each component. As shown in aurora_white, cg_sunflower, and vch_golden_yellow, diffusive base colors and highlights are reasonably separated into diffuse and specular components.

Fig. 4 shows the PSNR of the previous method [26], our Fresnel model, and our diffraction model. Our Fresnel model outperforms the previous model 35 materials out of 51 isotropic BRDFs, and our diffraction model outperforms 49 out of 51 in terms of PSNR. As shown in the graph, compared to Fresnel and previous models, the diffraction model improves PSNR especially for cc materials and vch materials that exhibit color-changing effects.

Fig. 5 shows the rendering results of cc_amber_citrine material where the diffraction model achieves the maximum improvement of PSNR compared to the previous model. As shown in Fig. 5, cc_amber_cirtine material exhibits complex specular reflections whose color changes from cyan (left), orange, to yellow (right). As shown in Fig. 5(b), the previous model cannot reproduce the color-changing effects. The Fresnel model (Fig. 5(c)(g)) can reproduce the cyan specular reflection but fails to reproduce yellow specular reflections. The diffraction model can reproduce such color-changing effects and the reddish circular reflections, as shown in Fig. 5 (d)(h).

Fig. 6 shows the rendering results of laika_ceiling_paint_18_gray material where the diffraction model is inferior to the previous model. It is conceivable that this waterborne paint material can violate our underlying assumption that the BRDF is modeled by the microfacet theory. In addition, since this material is matte and the diffuse component of our two models is the same as that of the previous model, the benefits of our method are negligible. While our two separation models are inferior to the previous model in this material, the visual difference between them is subtle, as shown in Fig. 6.

5.2 Specular component separation

Our method further decomposes the specular component into the Fresnel effect that depends on the difference angle θ_d and the diffraction effect depending on the half angle θ_h and θ_d. Fig. 7 shows the separation of the specular component. Our method can extract characteristic circular reflections for irid materials (top three rows) as shown in Fig. 7 (d).

Table 1: Average PSNR, SSIM, MAPE, and relMSE of each separation method.

method	PSNR↑	SSIM↑	MAPE↓	relMSE↓
Previous metod [26]	43.60	0.9887	7.36%	0.0218
Ours (Fresnel model)	45.72	0.9898	6.52%	0.0141
Ours (diffraction model)	52.11	0.9945	3.29%	0.0034

Table 2: Average PSNR, SSIM, MAPE, and relMSE of analytic model and our diffraction model in Fig. 8.

method	PSNR↑	SSIM↑	MAPE↓	relMSE↓
analytic model	31.72	0.9570	12.84%	0.0326
Ours (diffraction model)	37.56	0.9643	4.73%	0.0054

For matte materials such as paper_yellow (fourth row) in Fig. 7, diffraction effects whose colors differ from the yellow color of the diffuse component can be seen. These effects can be seen in the underlying diffraction microfacet BRDF and materials such as light-red-paint, white-marble, and yellow-phenolic materials in the MERL BRDF dataset (please see the supplemental material [12]). For specular materials such as satin_blue material (fifth row), additional glossy reflections can be seen in Fig. 7(d), which also can be seen in the underlying diffraction microfacet BRDF (e.g., gold_metallic_paint2 material in the supplemental material [12]). Organic materials such as leaf_mape material (sixth row in Fig 7) exhibit subtle diffraction effects, which can be seen in fruitwood-241 material of the supplemental material [12].

5.3 Comparison with analytic model fitting

We compare our diffraction model with analytic BRDF model in Fig. 8. Our method fits the EPFL BRDF dataset with microfacet BRDF (GGX normal distribution function). Our method calculates the parameters α_d and α_s in Sec. 4.2 for each wavelength using the non-linear optimization library Ceres solver.

As shown in Fig. 8, our diffaction model can produce goniochromatic effects for cc_amber_citrine (second row) and cc_iris_purple_gem (third row). In addition, characteristic circular reflections in irid_flake_paint2 (fourth row) can be reproduced by using our model, while GGX microfacet BRDF fails to reproduce such complex reflections. While separating diffuse and specular components for analytic models are trivial, fitting measured BRDFs with analytic models requires costly non-linear optimization, and the rendering results of our separation model are superior to those of GGX microfacet model as shown in Fig. 8. Table. 2 shows statistics on errors of analytic model and our diffraction model in Fig. 8. As shown in Table. 2, our diffraction model increases the PSNR by about 6 dB on average, and our model achieves better PSNR for 47 materials out of 51 materials.

6 Discussion and Limitation

While our separation models can reproduce color-changing effecs, our method has several limitations. Since our two separation models base microfacet BRDFs, materials that do not meet the underlying model (e.g., layered materials) cannot be well represented. Fig. 9 shows the failure case of our method for cc_green_marachite material that exhibits circular reddish highlights. In Fig. 9 (b), the previous method cannot represent the yellowish specular reflection. The Fresnel model can reproduce such specular reflection, as shown in Fig. 9(c), but it lacks the circular reddish reflections in the reference image. The diffraction model struggles to represent the circular reflections but fails, as shown in Fig. 9 (c).

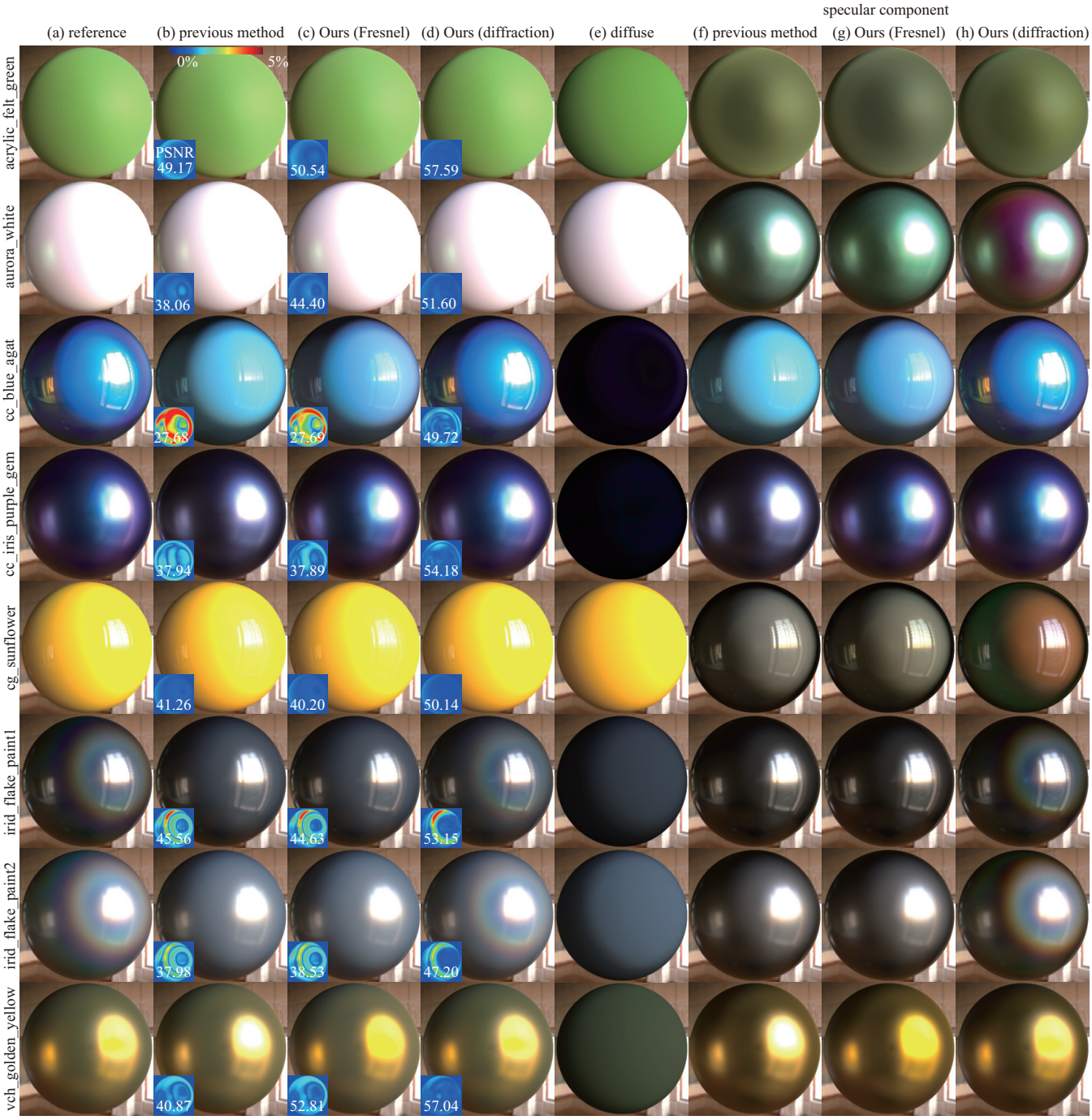

Figure 3: Comparison between the previous method [26] and our two separation models. From left to right, (a) reference image rendered with the original BRDF, (b) rendered with the previous method [26], (c) our Fresnel model, (d) our diffraction model, (e) the diffuse component, (f) the specular component of the previous method [26], (g) the specular component of our Fresnel model, (h) the specular component of our diffraction model. The inset images visualize the mean absolute percentage error (MAPE). As shown in these images and the PSNR values, our method can improve the accuracy of the separation models.

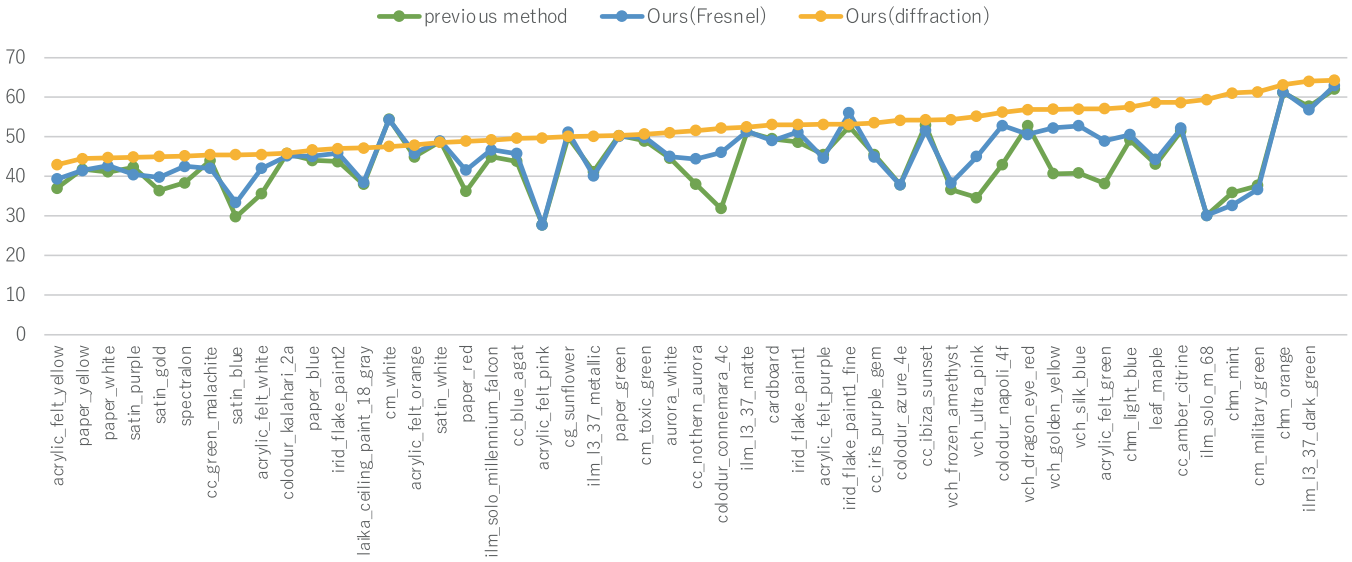

Figure 4: PSNR of 51 EPFL BRDFs. The Fresnel model achieves better PSNR for 35 materials, and the diffraction model improves PSNR for 49 materials out of 51 materials.

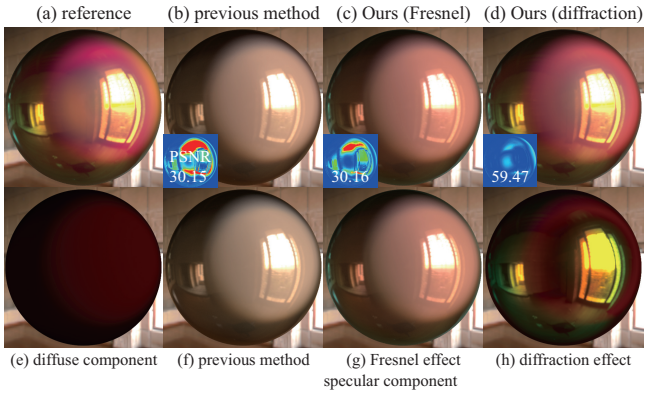

Figure 5: Rendering results of cc_amber_citrine material where our diffraction model improves PSNR up to 29.32 dB compared to the previous method [26]. Our diffraction model can represent complex reflections.

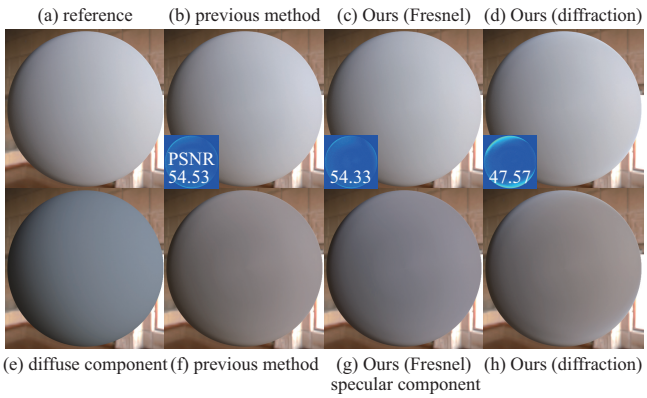

Figure 6: Rendering results of laika_ceiling_paint_18_gray material where the previous method [26] outperforms our diffraction model. While our method is inferior in this case, the visual difference is subtle.

Since the spectral distribution of our Fresnel model $s_s(\theta_d, \lambda)$ is two-dimensional and that of our diffraction model $s_s(\theta_h, \theta_d, \lambda)$ is three-dimensional, the data size of each material of our separation model is larger than that of the previous method [26]. The data size c_s for spectral measured BRDF is 2 KB (double precision), while that for $s_s(\theta_d, \lambda)$ and $s_s(\theta_h, \theta_d, \lambda)$ are 140 KB and 12.6 MB, respectively. The total data size, including the directional components $\rho_d(\omega_i, \omega_o)$ and $\rho_s(\omega_i, \omega_o)$ for the previous method, our Fresnel model, and our diffraction model per material is about 23.4 MB, 23.6 MB, and 36 MB, respectively. One possible solution to compact representation is to encode each component with a neural network such as Neural BRDF [27].

7 Conclusions

We have presented a diffuse-specular separation method for measured spectral BRDFs. In contrast to the previous separation model that represents the specular component with a single, direction-independent color term, our method can represent color-changing effects based on the Fresnel term in the microfacet BRDF model. We also presented the diffraction model that is based on the diffraction microfacet BRDF model. Our diffraction model can capture complex lighting effects and improves PSNR by about 10 dB on average and up to 30 dB in the EPFL BRDF dataset compared with the previous separation model. Our diffraction model improves PSNR by about 6 dB on average compared with microfacet BRDF model.

Currently, the directional components and the diffraction model require several megabytes per material, which would be problematic for some rendering applications. We would like to compress our separation model using neural network in future work. In addition, we would like to edit each reflection component to enhance the practicality of measured BRDFs.

References

[1] M. M. Bagher, J. Snyder, and D. Nowrouzezahrai. A non-parametric factor microfacet model for isotropic BRDFs. *ACM Trans. Graph.*, 35(5):159:1–159:16, 2016.

[2] S. Bako, T. Vogels, B. Mcwilliams, M. Meyer, J. Novák, A. Harvill, P. Sen, T. Derose, and F. Rousselle. Kernel-predicting convolutional networks for denoising monte carlo renderings. *ACM Trans. Graph.*, 36(4):97:1–97:14, 2017.

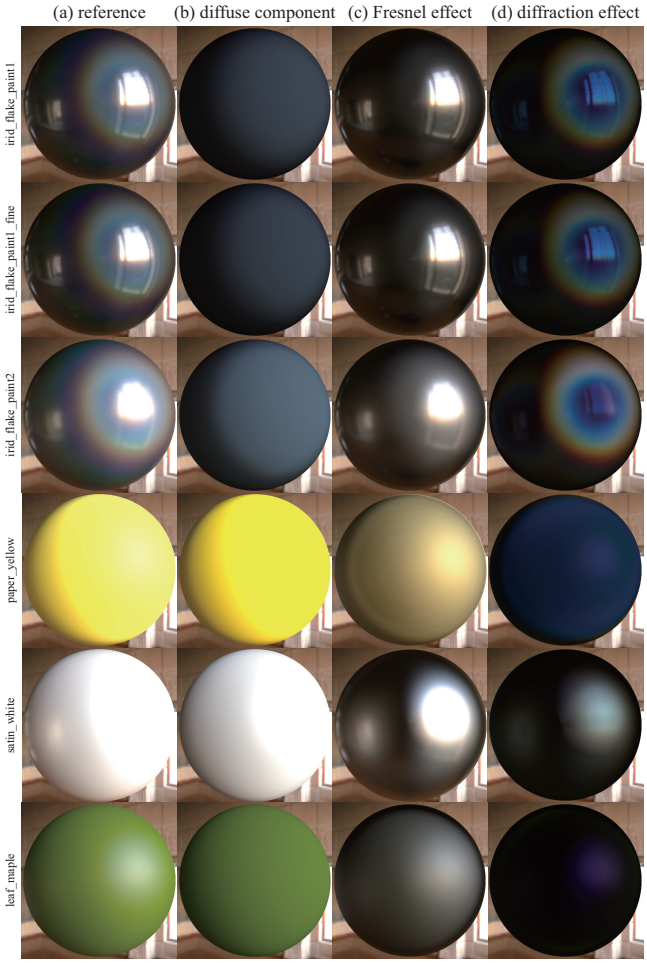

Figure 7: Specular component separation of irid_flake_paint1, irid_flake_paint1_fine, irid_flake_paint2, paper_yellow, satin_white, and leaf_maple materials. Characteristic circular reflections in irid materials can be separated by using our method. Glossy reflections shown in the previous method [12] can be seen in (d).

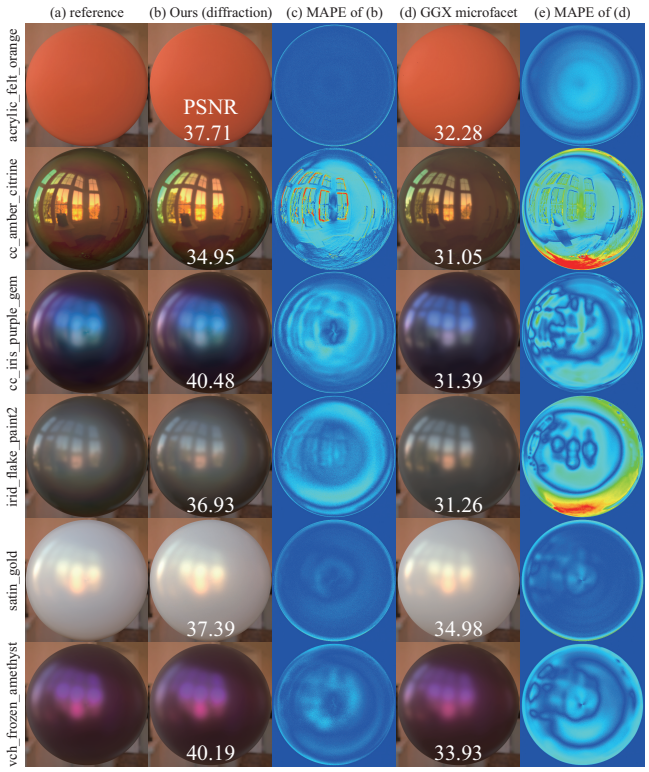

Figure 8: Comparison with fitted analytic BRDF model (GGX microfacet BRDF). Our diffraction model can reproduce complex lighting effects in cc_amber_citrine, cc_iris_purple_gem, and irid_flake_paint2 while fitted analytic model fails to reproduce.

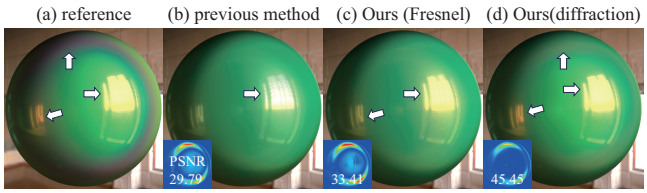

Figure 9: Failure case of our separation. Our method cannot represent reddish reflections shown in cc_green_marachite material. This material exhibit complex change of specular reflections, orange specular reflection (left) to yellow specular reflection (right), and circular reddish reflections. The Fresnel model can reproduce yellow specular reflection, but fail to reproduce the color of left specular reflection. The diffraction model can reproduce both colors of specular reflections, but fails to reproduce circular reddish reflection.

[3] L. Belcour and P. Barla. A practical extension to microfacet theory for the modeling of varying iridescence. *ACM Trans. Graph.*, 36(4):65:1–65:14, 2017.

[4] J. Bieron and P. Peers. An adaptive BRDF fitting metric. *Computer Graphics Forum*, 39(4):59–74, 2020.

[5] A. Bilgili, A. Öztürk, and M. Kurt. A general BRDF representation based on tensor decomposition. *Computer Graphics Forum*, 30(8):2427–2439, 2011.

[6] R. L. Cook and K. E. Torrance. A reflectance model for computer graphics. *ACM Trans. Graph.*, 1(1):7–24, 1982.

[7] J. Dupuy, E. Heitz, J.-C. Iehl, P. Poulin, and V. Ostromoukhov. Extracting microfacet-based BRDF parameters from arbitrary materials with power iterations. *Computer Graphics Forum*, 34(4):21–30, 2015.

[8] J. Dupuy and W. Jakob. An adaptive parameterization for efficient material acquisition and rendering. *ACM Trans. Graph.*, 37(6):274:1–274:14, 2018.

[9] J. Filip and R. Vávra. Template-based sampling of anisotropic BRDFs. *Computer Graphics Forum*, 33(7):91–99, 2014.

[10] E. Garces, C. Rodriguez-Pardo, D. Casas, and J. Lopez-Moreno. A survey on intrinsic images: Delving deep into lambert and beyond. *International Journal of Computer Vision*, 130(3):836–868, 2022.

[11] J. Guo, Z. Zong, Y. Song, X. Fu, C. Tao, Y. Guo, and L.-Q. Yan. Efficient light probes for real-time global illumination. *ACM Trans. Graph.*, 41(6):202:1–202:14, 2022.

[12] N. Holzschuch and R. Pacanowski. A two-scale microfacet reflectance model combining reflection and diffraction. *ACM Trans. Graph.*, 36(4):66:1–66:12, 2017.

[13] B. Hu, J. Guo, Y. Chen, M. Li, and Y. Guo. DeepBRDF: A deep representation for manipulating measured BRDF. *Computer Graphics Forum*, 39(2):157–166, 2020.

[14] J. Kautz and M. McCool. Interactive rendering with arbitrary BRDFs using separable approximations. In *Eurographics Workshop on Rendering*, pp. 281–292, 1999.

[15] A. Krywonos. *Predicting Surface Scatter using a Linear Systems Formulation of Non-Paraxial Scalar Diffraction*. PhD thesis, University of Central Florida, 2006.

[16] L. Latta and A. Kolb. Homomorphic factorization of BRDF-based lighting computation. In *Proceedings of the 29th Annual Conference on Computer Graphics and Interactive Techniques*, pp. 509–516, 2002.

[17] J. Lawrence, A. Ben-Artzi, C. DeCoro, W. Matusik, H. Pfister, R. Ramamoorthi, and S. Rusinkiewicz. Inverse shade trees for non-parametric material representation and editing. *ACM Trans. Graph.*, 25(3):735–745, 2006.

[18] J. Lawrence, S. Rusinkiewicz, and R. Ramamoorthi. Efficient BRDF importance sampling using a factored representation. *ACM Trans. Graph.*, 23(3):496–505, 2004.

[19] J. Löw, J. Kronander, A. Ynnerman, and J. Unger. BRDF models for accurate and efficient rendering of glossy surfaces. *ACM Trans. Graph.*, 31(1):9:1–9:14, 2012.

[20] W. Matusik, H. Pfister, M. Brand, and L. McMillan. A data-driven reflectance model. *ACM Trans. Graph.*, 22(3):759–769, 2003.

[21] M. D. McCool, J. Ang, and A. Ahmad. Homomorphic factorization of BRDFs for high-performance rendering. In *Proceedings of the 28th Annual Conference on Computer Graphics and Interactive Techniques*, pp. 171–178, 2001.

[22] A. Ngan, F. Durand, and W. Matusik. Experimental analysis of BRDF models. In *Proceedings of the Sixteenth Eurographics Conference on Rendering Techniques*, pp. 117–126, 2005.

[23] J. B. Nielsen, H. W. Jensen, and R. Ramamoorthi. On optimal, minimal BRDF sampling for reflectance acquisition. *ACM Trans. Graph.*, 34(6):186:1–186:11, 2015.

[24] M. Ribardière, B. Bringier, D. Meneveaux, and L. Simonot. Std: Student's t-distribution of slopes for microfacet based bsdfs. *Computer Graphics Forum*, 36(2):421–429, 2017.

[25] C. Soler, K. Subr, and D. Nowrouzezahrai. A versatile parameterization for measured material manifolds. *Computer Graphics Forum*, 37(2):135–144, 2018.

[26] T. Sun, H. W. Jensen, and R. Ramamoorthi. Connecting measured BRDFs to analytic BRDFs by data-driven diffuse-specular separation. *ACM Trans. Graph.*, 37(6):273:1–273:15, 2018.

[27] A. Sztrajman, G. Rainer, T. Ritschel, and T. Weyrich. Neural BRDF representation and importance sampling. *Computer Graphics Forum*, 40(6):332–346, 2021.

[28] B. Walter, S. R. Marschner, H. Li, and K. E. Torrance. Microfacet models for refraction through rough surfaces. In *Proceedings of the 18th Eurographics Conference on Rendering Techniques*, pp. 195–206, 2007.

[29] J. Wang, P. Ren, M. Gong, J. Snyder, and B. Guo. All-frequency rendering of dynamic, spatially-varying reflectance. *ACM Trans. Graph.*, 28(5):1–10, 2009.

[30] C. Zheng, R. Zheng, R. Wang, S. Zhao, and H. Bao. A compact representation of measured BRDFs using neural processes. *ACM Trans. Graph.*, 41(2):14:1–14:15, 2021.